Bulletin of the Seismological Society of America, Vol. 102, No. 3, pp. 1266–1275, June 2012, doi: 10.1785/0120110149

Ⓔ

Short Note

Test of a Threshold-Based Earthquake Early-Warning Method Using Japanese Data

by Simona Colombelli, Ortensia Amoroso, Aldo Zollo, and Hiroo Kanamori

Abstract Most of existing earthquake early-warning systems are regional or on-site systems. A new concept is the integration of these approaches for the definition of alert levels and the estimation of the earthquake potential damage zone (PDZ). The key element of the method is the real-time, simultaneous measurement of initial peak displacement (P_d) and period parameter (τ_c) in a 3-s window after the first *P*-wave arrival time at accelerometer stations located at increasing distances from the epicenter. As for the on-site approach, the recorded values of P_d and τ_c are compared to threshold values, which are set for a minimum magnitude M 6 and instrumental intensity I_{MM} VII, according to empirical regression analysis of strong-motion data from different seismic regions. At each recording site the alert level is assigned based on a decisional table with four entries defined by threshold values of the parameters P_d and τ_c. A regional network of stations provides the event location and transmits the information about the alert levels recorded at near-source stations to more distant sites, before the arrival of the most destructive phase.

We present the results of performance tests of this method using ten $M > 6$ Japanese earthquakes that occurred in the period 2000–2009 and propose a very robust methodology for mapping the PDZ in the first seconds after a moderate-to-large earthquake. The studied cases displayed a very good matching between the rapidly predicted earthquake PDZ inferred from initial *P*-peak displacement amplitudes and the instrumental intensity map, the latter being mapped after the event, using peak ground velocity and/or acceleration, or from field macroseismic surveys.

Online Material: Animated GIF files of simulations of the threshold-based method.

Introduction

During the last three decades, the improvement of technology has made it possible to implement earthquake early-warning systems (EEWS) in many active seismic regions of the world. Operational EEWS are actually running in Japan (Nakamura, 1984, 1988; Odaka *et al.*, 2003; Horiuchi *et al.*, 2005), Taiwan (Wu and Teng, 2002; Wu and Zhao, 2006), and Mexico (Espinosa-Aranda *et al.*, 2009), while other systems are under testing or development in California (Allen and Kanamori, 2003; Allen, Brown, *et al.* 2009; Allen, Gasparini, *et al.* 2009; Böse *et al.*, 2009), Turkey (Alcik *et al.*, 2009), Romania (Böse *et al.*, 2007), and China (Peng *et al.*, 2011). In southern Italy, the PRobabilistic and Evolutionary early warning SysTem (PRESTo), monitoring the Apenninic fault system (which is causative of frequent moderate-to-large earthquakes), has been operational for testing on small-to-moderate size events since December 2009 (Zollo, Iannaccone, Lancieri, *et al.*, 2009; Zollo, Iannaccone, Convertito, *et al.*, 2009; Satriano *et al.*, 2010).

Two different configurations for EEWS are mainly developed: regional (or network-based) and on-site (or station-based). In a regional EEWS, the early portion of recorded signals is used to rapidly estimate source parameters (event location and magnitude) and to predict a ground-motion intensity measure (peak ground velocity [PGV] or peak ground acceleration [PGA]) at distant sites by using an existing, empirical ground-motion prediction equation. In such a configuration, a continuously updated and refined estimation of source parameters is released in real time as new data are acquired by the network, and the lead time (the time between the alert issue and the arrival of damaging waves at the target site) is relatively long, depending on the source-to-site distance. In an on-site EEWS, peak amplitude and/or

predominant period measurements on the early portion of recorded *P* signals are generally used to predict the ensuing peak ground motion at the same site. In this configuration, the alert for an impending earthquake damage at the target site is issued based mainly on a local measurement of *P*-wave ground motion, bypassing the uncertain estimation of earthquake location and magnitude or the prediction of the ground-shaking level through an empirical attenuation law. An ideal system should provide large enough lead times, accurate estimations of source parameters, and reliable predictions of the expected ground motion at the target.

In a very recent paper, Zollo *et al.* (2010) proposed a seismic alert methodology that integrates the approaches of regional and on-site EEWS. The procedure is based on the real-time, joint measurement of initial peak displacement (P_d) and period parameter (τ_c) in a 3-s window after the first *P* arrival time and on the use of P_d as a proxy for PGV (Wu and Kanamori, 2005, 2008). The on-site warning is issued based on the matching of the recorded values of P_d and τ_c to prior established threshold values. Based on local measurements, the system can rapidly distinguish a potentially damaging from nondamaging earthquake and, if needed, issue an alert in the epicentral area and distant sites. The network of stations in the source area produces the event location and transmits the information about the alert levels recorded at near-source stations to more distant sites, before the arrival of the most destructive phase, as in a regional early-warning system.

In this short note, we present the results of performance tests of this method and propose a new methodology for a real-time mapping of the potential damage zones (PDZ) in the first seconds after a moderate-to-large earthquake. The methodology has been applied off-line to the strong-motion records of a set of ten $M > 6$ earthquakes that occurred in Japan during the last decade; the results demonstrate the method's efficiency and rapidity for issuing an early warning and mapping the damage zone in a few seconds after the earthquake occurrence.

Data and Method

For this study we selected ten large Japanese earthquakes that occurred from 2000 to 2009 (Table 1). Using the Japan Meteorological Agency (JMA) catalog, events having a magnitude greater than 6 on a JMA magnitude scale have been selected. The waveforms have been extracted from the KiK-net and K-NET databases (see Data and Resources); the analyzed data set consists of 1341, three-component strong-motion accelerometer records. Figure 1 shows the distribution of selected events and used stations. The preliminary procedure of data analysis first involves removal of the mean value and linear trend and then manual *P* picking on the vertical component of accelerometer records. Accelerometer records are then integrated once to get velocity records; a second integration is performed to obtain displacement and a causal Butterworth high-pass filter with a cut-off frequency of 0.075 Hz and two poles is finally applied to remove the long-period drift after the double integration. The events have been located using the real-time location methodology of Satriano *et al.* (2008) in the layered velocity model proposed by Ueno *et al.* (2002). The P_d has been measured on the vertical component of high-pass filtered displacement trace within a 3-s time window after the *P* picking; the estimation of τ_c requires displacement and velocity traces in the same seismogram window. The method we applied in this work has been described in the recent paper of Zollo *et al.* (2010); for the sake of completeness we briefly summarize it here.

By analyzing strong-motion data from modern accelerometer networks in Japan, Taiwan, and Italy and considering a maximum epicentral distance of 60 km, Zollo *et al.* (2010) derived the relation between the initial peak ground displacement (P_d) and the PGV:

$$\log(\mathrm{PGV}) = 0.73(\pm 0.01) \times \log(P_d) + 1.30(\pm 0.02), \quad (1)$$

where P_d is measured in centimeters, PGV in centimeters per second, and the standard error is 0.41.

From the comparison with observed intensity maps for some significant Californian earthquakes, Wald *et al.* (1999) defined the instrumental intensity (I_{MM}), which relates the recorded peak acceleration and velocity amplitudes to the expected damage distribution. The instrumental intensity is currently used by the U.S. Geological Survey in the ShakeMap generation procedure. Given the relationship from Wald *et al.* (1999) and the observed correlation of P_d with PGV, the

Table 1
List of Events Used in This Work

Name of Earthquake	Origin Time (UTC) (yyyy/mm/dd hh:mm:ss)	Latitude (° N)	Longitude (° E)	Depth (km)	M_{JMA}
Western Tottori	2000/10/06 04:30:32.69	35.29	133.35	10.44	7.3
Geiyo	2001/03/24 06:28:09.49	34.13	132.70	46.19	6.7
Miyagi-Oki	2003/05/26 09:24:48.49	38.82	141.67	70.02	7.1
Chuetsu	2004/10/23 08:56:15.14	37.29	138.86	12.77	6.8
Chuetsu Aftershock	2004/10/23 09:12:11.22	37.27	138.80	12.47	6.0
Fukuoka	2005/03/20 01:53:05.20	33.75	130.17	13.39	7.0
Noto Hanto	2007/03/25 00:42:13.22	37.20	136.73	10.67	6.9
Chuetsu-Oki	2007/07/16 01:13:37.62	37.52	138.64	16.62	6.8
Iwate–Miyagi	2008/06/13 23:44:00.25	39.03	140.89	5.39	7.2
Shizuoka	2009/08/10 20:07:20.52	34.77	138.50	25.15	6.5

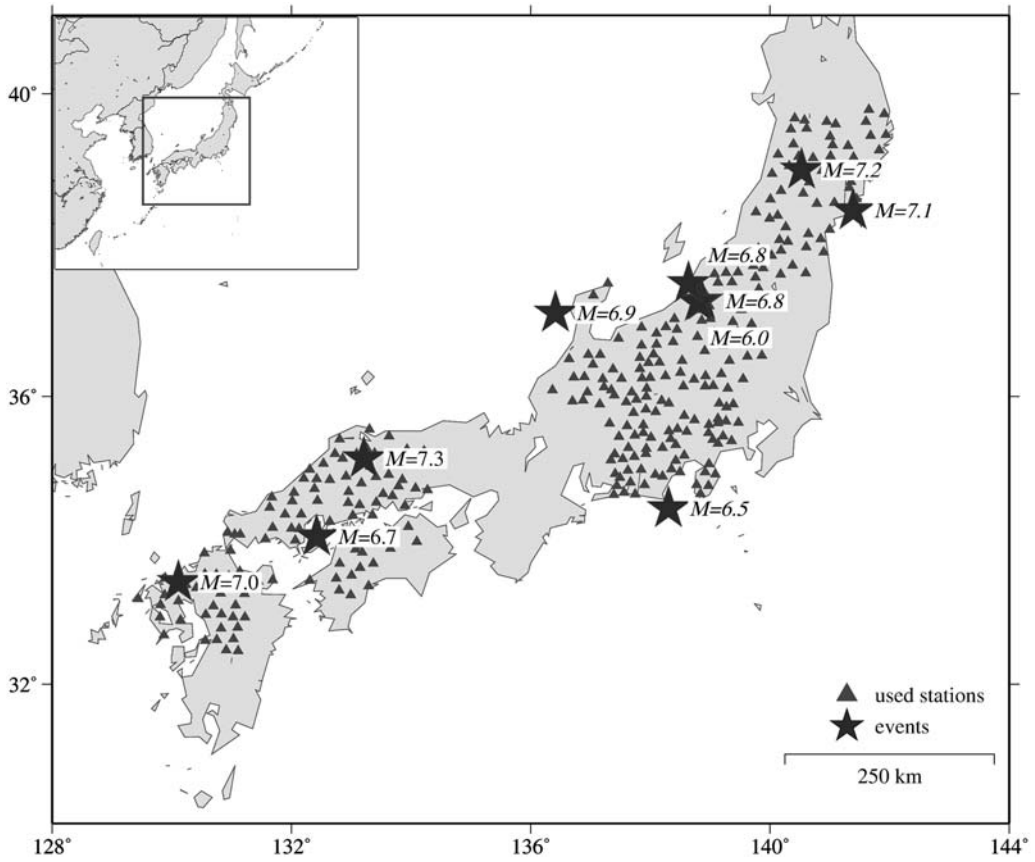

Figure 1. Distribution of events and of KiK-net and K-NET stations used in this work.

potential damaging effect of an earthquake can be rapidly predicted from the real-time measurement of peak displacement on the initial *P*-wave train.

With the same data set Zollo *et al.* (2010) determined the relationship between the period parameter τ_c and magnitude in the range $4 < M < 8.3$; the best-fit regression line has been derived on average binned data ($\Delta M = 0.3$) weighted by the standard deviation for data in each bin. They found

$$\log(\tau_c) = 0.21(\pm 0.01) \times M - 1.19(\pm 0.08), \qquad (2)$$

where τ_c is measured in seconds and the standard error is 0.25.

With the aim of inferring a rapid estimation of the extent of the PDZ, the empirical relationship that relates P_d, τ_c, and hypocentral distance (R) has been therefore determined. Given the observed dependency of the period parameter with magnitude, this relationship is similar to a ground-motion prediction equation for the parameter P_d in the investigated range of distances. Through a multivariate linear regression analysis, the best fitting procedure provided

$$\log(P_d) = 1.93(\pm 0.03) \times \log(\tau_c) - 1.23(\pm 0.09) \times \log(R) + 0.6(\pm 0.1), \qquad (3)$$

where R is measured in kilometers, τ_c in seconds, P_d in centimeters, and the standard error is 0.7.

A threshold-based system requires the definition of alert levels, which are set depending on *a priori* values for the real-time measured ground-motion parameters. Using the previous empirical relationships, four alert levels (0, 1, 2, and 3) are defined for the measured values of the parameters P_d and τ_c at a given site (Fig. 2). The threshold values for the alert levels have been chosen in order to have the maximum alert level (level 3) for an earthquake with predicted magnitude $M \geq 6$ and with an instrumental intensity $I_{MM} \geq$ VII. In particular, the P_d threshold (0.2 cm) is set from equation (1) using the PGV value corresponding to $I_{MM} =$ VII and allowing for the estimated 1-σ error bounds on the PGV versus P_d relationship; the τ_c threshold (0.6 s) is set from equation (2) using $M = 6$, allowing for the 1-σ error bounds. The alert table is derived from the original scheme proposed by Wu and Kanamori (2005) and can be interpreted in terms of potential damaging effects near the recording station and far away from it. In case of an alert level 3 ($\tau_c \geq 0.6$ s and $P_d \geq 0.2$ cm), the earthquake is likely to have a large size and to be located close to the recording site; thus we expect a high level of damage both nearby and far from the station. For an alert level 1 ($\tau_c \geq 0.6$ s and $P_d < 0.2$ cm), the event is likely to have a large size but occur far from the station; thus damage is expected only far away from the recording

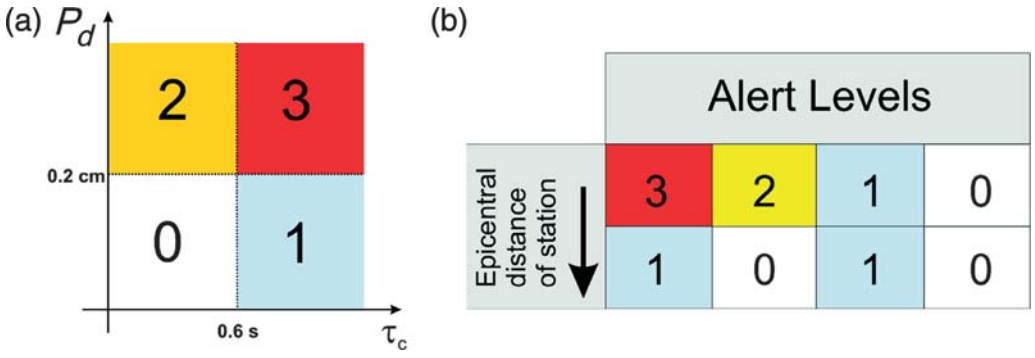

Figure 2. Alert levels and threshold values for observed early-warning parameters (Zollo *et al.*, 2010). (a) P_d versus τ_c diagram showing the chosen threshold values and the regions delimiting the different alert levels: level 3, damage expected nearby and far away from the station; level 2, damage expected only near the station; level 1, damage expected only far away from the station; level 0, no expected damage. (b) Expected variation of alert levels as a function of the epicentral distance: the allowed transitions between alert levels are those from 3 to 1 and from 2 to 0.

site. In case of an alert level 2 ($\tau_c < 0.6$ s and $P_d \geq 0.2$ cm), the size of the event is likely to be small, but the event occurs close to the station; thus earthquake effects are expected only near the recording site. Finally, if the alert level is 0 ($\tau_c < 0.6$ s and $P_d < 0.2$ cm), no damage is expected either close or far away from the station.

As soon as a series of measurements of P_d and τ_c are available, using the average τ_c value and fixing P_d at its threshold value, equation (3) can be used to determine the radius (R in equation 3) of the PDZ, that is the area within which the highest intensity values are expected to be observed. In this short note we generalize this methodology to the real-time estimation of the PDZ based on the combined use of measured and predicted ground-motion values. The area covered by stations is divided into cells by using a pre-fixed spatial grid, which is needed to fill the gaps where stations are not available. At those stations where the first 3 s of signal after the P picking are available, an alert level is locally assigned, based on P_d and τ_c measurements. At the same time, the event location is obtained by using the available P picks and RTLoc method. Furthermore, the expected P_d value can be predicted at each node of the grid, through equation (3) and the τ_c averaged over the available measurements at the considered time step. Measured and predicted P_d values are thus interpolated; the area within which the highest level of damage is expected can be delimited by the isoline corresponding to $P_d = 0.2$ cm.

Moreover, the expected PGV values at triggered stations and at grid nodes can be computed using equation (1) and finally converted into an instrumental intensity measure using the relationship of Wald *et al.* (1999). Once again, an interpolation is performed between all intensity values, and results can be plotted as a real-time, continuously updated, intensity map. This routine is repeated every second; as the waves propagate within the area and trigger other stations, the event location is refined by using P pickings, average τ_c value is updated, other alert levels are defined, and more data are used for the interpolation procedure.

Application and Results

We applied the proposed methodology to the ten selected events of the Japanese strong-motion database. Figure 3 shows an example of ground-motion measurements and alert levels assigned at each recording station after P_d and τ_c measurements for the M 6.8, 2007 Chuetsu-Oki earthquake. For all the analyzed earthquakes, τ_c values do not show any dependence on distance, as expected from the previous works (e.g., Kanamori, 2005), at least in the analyzed range of distances (maximum epicentral distance, 200 km). The initial amplitude P_d instead generally decreases with the distance, due to the geometrical spreading and anelastic attenuation effects. As a consequence, the alert levels are maximum in near-source areas and decrease far away from the epicenter. Moreover, when the distance increases, the only transitions allowed between alert levels are those from 3 to 1 and from 2 to 0. All the other transitions are forbidden because they would imply a variation of the earthquake magnitude as a function of distance. The analyzed earthquakes confirmed that only transitions from alert level 3 to 1 are observed for moderate-to-large earthquakes, recorded by a network extending from the epicentral area to further distances. In this work the transition from 2 to 0, which is expected for small but strongly felt earthquakes (magnitude around 4), has never been observed.

For a complete and effective visualization of results, we decided to represent them through three maps: an instrumental intensity (I_{MM}) map and a JMA instrumental intensity (I_{JMA}) map, both of which provide information about the felt ground shaking, and an operative map that shows the distribution of alert levels and the predicted PDZ. Examples of snapshot maps are reported in Figure 4. Ⓔ All the snapshots resulting from the application of the threshold-based method to the selected events are available as an electronic supplement to this paper. Each snapshot shows the comparison between the I_{MM}, the I_{JMA}, and the PDZ map at increasing times, starting from the first P pick.

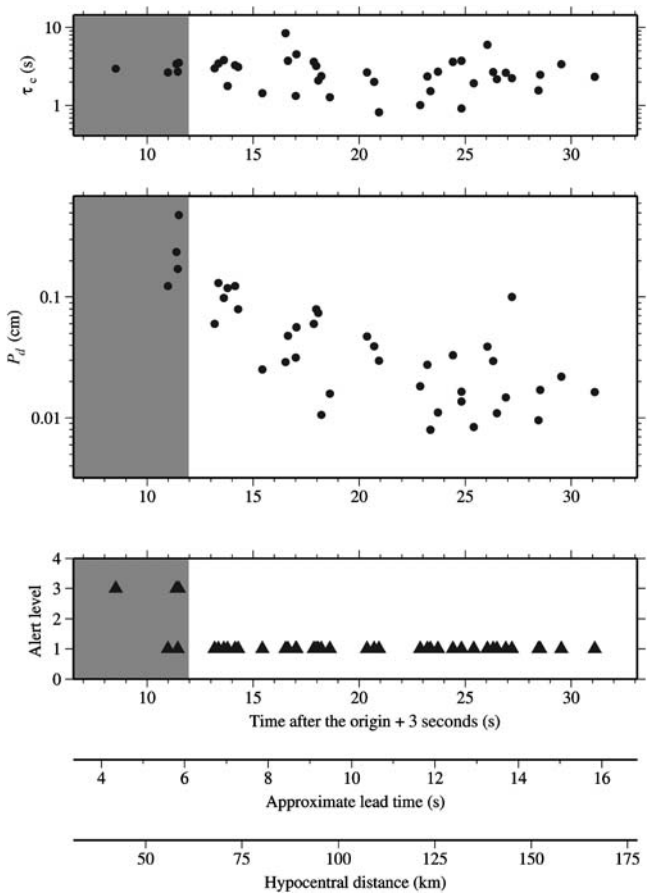

Figure 3. Time evolution of ground-motion measurements and the corresponding alert levels at the different stations, located at increasing distances from the epicenter of the 2007, M 6.8 Chuetsu-Oki earthquake. In each plot, points represent the recorded values at the considered stations: (top to bottom) the parameter τ_c, the initial peak ground displacement P_d, and the alert levels. Along the x axis the time at which each measurement is available is given. Time is counted starting from the origin time of the event and contains the 3 s necessary for data processing. As expected, P_d generally decreases with the increasing distance; the measured values of τ_c do not show any dependence on distance. The final plot shows the alert level that would have been issued at each station: they are maximum in near-source area and decrease with distance. Gray and white zones indicate the alert levels 3 and 1, respectively. The plot assumes no delay caused by telemetry/processing, which can be estimated around 1–3 s for computing and data transmission system.

The I_{JMA} scale was introduced in Japan in the early 1990s and is obtained on the vector composition of three-component ground-motion records by evaluating the total duration of PGA exceeding a reference value (Karim and Yamazaki, 2002). A value equal to 4 on the Japanese scale approximately corresponds to V or VI on the modified Mercalli scale, while 5 corresponds to VI or VII on the modified Mercalli scale (Kunugi, 2000).

The application of the method to the selected Japanese events confirmed the satisfactory performances of a threshold-based system for early-warning procedures: the visual matching between the real-time PDZ and the postevent I_{JMA} maps suggests that the PDZ reproduces with a good approximation the area within which the highest intensity values are observed. The $P_d = 0.2$ cm isoline (represented in Fig. 4 by the color transition from light blue to red) approximately corresponds to a I_{JMA} around 5, the minimum intensity necessary to issue a public warning. The agreement is even more robust when considering that the I_{JMA} map has been obtained from an independent data set Japan Meteorological Agency (2010).

Although it is known that I_{JMA} intensity measures may not always be a good indicator of damage, we introduced the I_{JMA} map with the aim of providing a further comparison of results of the proposed methodology and in order to make it suitable to Japan, for which the application has been conceived.

The three maps represented in Figure 4 for each event are essentially derived from different ground-motion quantities (PGV and PGA for I_{MM} and I_{JMA}, respectively, and P-wave peak displacement for the PDZ map). The comparison between I_{MM} and I_{JMA} intensity maps in Figure 4 is a useful test, although it should be noted that several factors make it difficult to evaluate the exact correspondence between the two scales. (a) The I_{JMA} map is the representation of a continuous quantity, while the I_{MM} intensity derives from the conversion of a continuous parameter (PGV) into a discrete scale; thus the boundary between two contiguous intensity values does not characterize in a rigorous way the effects of an earthquake and the perceived level of damage. (b) The empirical relationship between the two intensity scales provided by Kunugi (2000) shows a good correspondence in the range $1 \leq I_{MM} \leq 6$, but the correlation becomes poorer for higher intensity values. (c) The two maps have been obtained with different data sets, so that the number and spatial density of measurement points vary for the two parameters, affecting the interpolation procedure.

A quantitative assessment of the method performance can be obtained by counting the number of successes and failures of the system. For such a purpose, we utilized the scheme of Table 2 to evaluate the correspondence between the recorded alert level and the real magnitude and intensity values. The definitions of successful, missed, and false alarms are based on the assumption that only level 3 to 1 and level 2 to 0 transitions are allowed (Fig. 2). Figure 5 shows the results obtained by counting successes and failures of the system for all the considered events: 87.4% of alert levels have been correctly assigned, 11.9% are false alarms, and 0.7% are missed alarms. The high percentage of successful alarms and the very small number of missed alarms represent the main results of our application. To understand the relevance of the false alarms percentage, we determined the difference between predicted intensity (I_{MM} = VII) and observed intensity value. The variance distribution is shown in Figure 5: 36% of false alarms correspond to an intensity value of VI, 52% to an intensity V, and 12% to intensity III. An intensity value of VI, although it does not correspond to the maximum alert level (3), is synonymous with an earthquake that can be perceived by the population and may

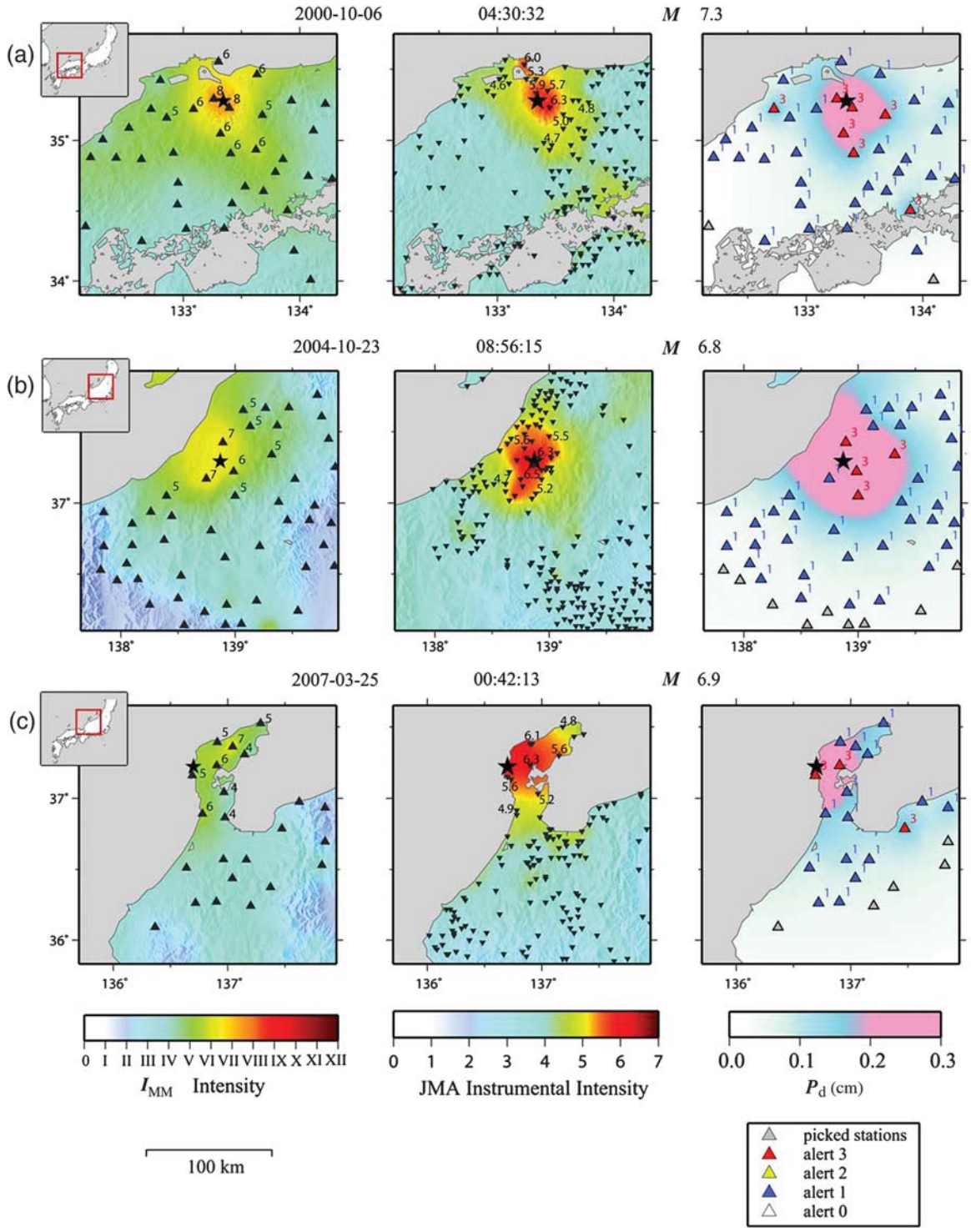

Figure 4. Off-line simulation of the threshold-based early-warning method for (a) 2007 *M* 7.3 Western Tottori earthquake, (b) 2004, *M* 6.8 Chuetsu earthquake, and (c) 2007 *M* 6.9 Noto Hanto earthquake. The figure shows examples of snapshot maps obtained by the procedure, as computed after that the initial *P* wave has been recorded at stations within 30–50 km from the epicenter. In each panel, the black star represents the epicenter, and the triangles indicate the used stations. (Left panel) The I_{MM} map, obtained by using the observed PGV values at K-NET and KiK-net stations. For the sake of uniformity we adopted the same color palette for all events; the color palette has been taken from the ShakeMap online manual (see Data and Resources). As a reference, values of measured I_{MM} intensity are reported for some stations in the epicentral area. (Center panel) The instrumental intensity, I_{JMA} map, as measured at JMA sites, is represented by the same color palette as the I_{MM} map but adapted from 0 to 7. As a reference, values of measured I_{MM} intensity are reported for some stations in the epicentral area. (Right panel) The operative early-warning map resulting from the interpolation of measured and predicted P_d values. Gray triangles represent the stations triggered by the earthquake, while red and blue triangles show the alert level recorded at each station, as soon as 3 s of signal after the *P* picking are available. The color transition from light blue to red delimits the PDZ.

Table 2
Definition of Successful, Missed, and False Alarms Based on the Recorded Alert Levels*

Recorded Alert Level	Successful Alarm	Missed Alarm†	False Alarm†
3	$I_{MM} \geq$ VII	n.d.	$I_{MM} <$ VII
2	$I_{MM} \geq$ VII	n.d.	$I_{MM} <$ VII
1	$I_{MM} <$ VII	$I_{MM} \geq$ VII	n.d.
0	$I_{MM} <$ VII	$I_{MM} \geq$ VII	n.d.

*Each recorded alert level corresponds to a successful, missed or false alarm, based on the observed values of intensity and on the assumption that only transitions from 3 to 1 and 2 to 0 between alert levels are allowed. For example, a recorded alert level 3 corresponds to a successful alarm if the observed intensity is ≥ VII and to a false alarm if the observed intensity is < VII. In the same way, the recorded alert level 1 can be a successful alarm if the observed intensity is < VII and a missed alarms if the observed intensity is ≥ VII. The alert levels 3 or 2 cannot be missed alarms, as well as 1 and 0 cannot be false alarms.

†n.d., not defined.

provoke some damage; keeping this in mind, the percentage of false alarms can be considered smaller.

Figure 6 shows the prediction error of peak ground velocity as a function of distance. It is generally distributed around 0 and remains stable with distance, showing an approximate standard deviation of ±0.75, as inferred from the histograms presented in the figure.

Finally, we discuss the results of the application of the threshold-based method to the 2008 Iwate–Miyagi earthquake. In this case we observed a large discrepancy between the extent of the maximum damaged area (as revealed by the I_{MM} and I_{JMA} maps) and the PDZ (as estimated from the threshold-based approach). The earthquake occurred at 23:44 (UTC), 13 June 2008 at 39.03° N, 140.89° E and 5.39 km depth. As shown in Figure 7, the PDZ resulting from the interpolation between measured and predicted P_d values, is much larger than the area in which the highest intensity values (both I_{MM} and I_{JMA}) are observed (Fig. 7a). Except for the Iwate–Miyagi earthquake, we did not encounter this problem for any other events listed in Table 1 (see also Ⓔ the electronic supplement to this paper). We then compared the measured values of P_d and τ_c with those predicted by the empirical attenuation relationship (equations 2 and 3). In Figure 7c, we plotted P_d and τ_c for the Iwate–Miyagi earthquake as a function of distance. The average τ_c value for this event (2.6 s) is slightly larger (almost 30%) than those expected for an M 7.2 earthquake (around 2 s) from the τ_c versus M relationship, while the observed P_d values are consistent with those predicted, except for some distant stations in the west–northwest direction (indicated with a circle) where the observed P_d values are a factor around 4 larger than the expected values. These overestimated P-peak displacement values are the cause for about twice the linear extension of PDZ in the west–northwest sector relative to the other azimuthal directions, where P_d values follow approximately the expected amplitude decay with distance. Because I_{MM} and I_{JMA}, which are intensity measurements derived from ground velocity and acceleration, do not show a similar pattern, the large P_d values observed at those sites could be due to a low-frequency amplification effect in this region that results in a larger PDZ relative to the damage zone, as inferred from the I_{MM} and I_{JMA} maps.

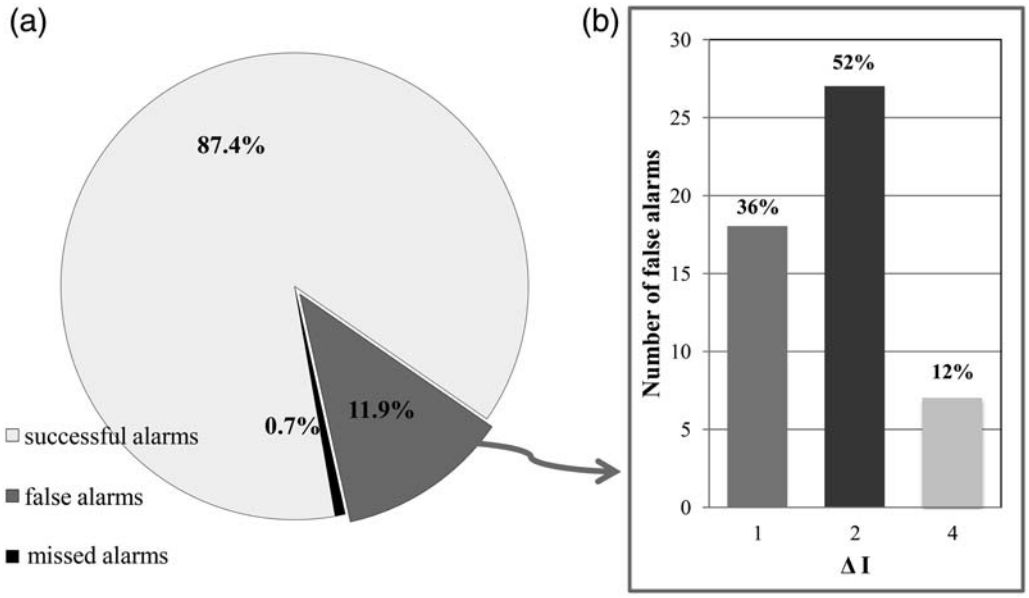

Figure 5. Distribution of successes and failures of the system. (a) The relative percentage of successful, false, and missed alarms, which are respectively 87.4%, 11.4%, and 0.7%. (b) In the histogram of false alarms, ΔI represents the difference between predicted (I_{MM} VII) and observed intensity values: 36% of false alert levels 3 correspond to an intensity value of VI; 52% correspond to intensity V, and 12% to intensity III.

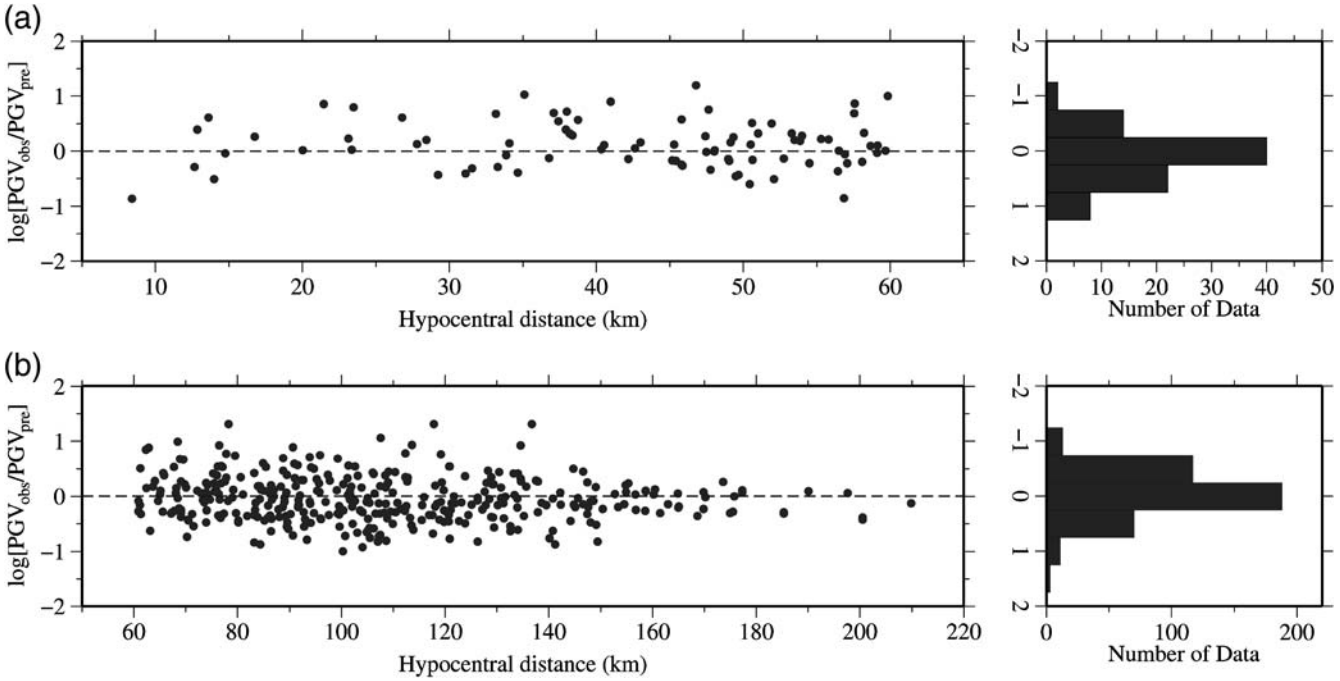

Figure 6. Prediction error shown as a function of hypocentral distance; (a) points within 60 km and (b) points beyond 60 km. The prediction error is clearly uncorrelated with distance, and points follow a Gaussian distribution with most of the data contained within a ± 0.25 interval around zero (dashed lines represent the zero value).

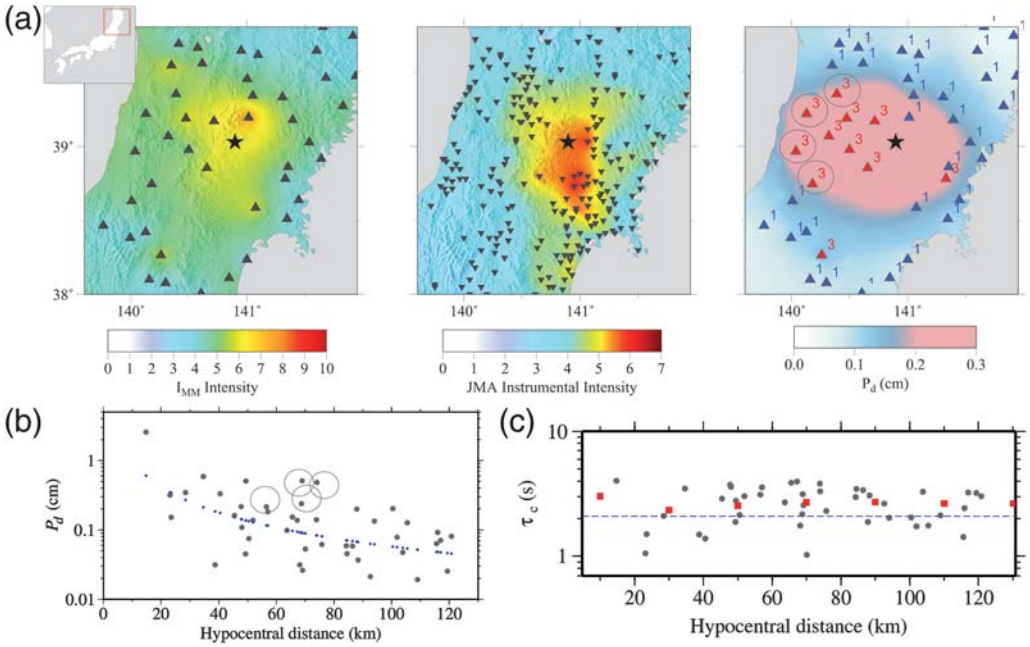

Figure 7. Results of the threshold-based method for the 2008, Iwate–Miyagi earthquake. (a) Snapshot map (refer to the caption of Figure 4): the PDZ resulting from the interpolation between measured and predicted P_d values is much larger than the area in which the highest intensity values are observed. Stations surrounded by a circle in the west–northwest direction are those for which the observed P_d values are a factor around 4 larger than the expected values. (b) Measured P_d values as a function of distance (gray dots) and the predicted P_d values (blue dots) based on the empirical attenuation relationship (equation 3) and on the expected τ_c value from the τ_c vs. M relationship (equation 2) for a magnitude 7.2 event. (c) τ_c values as a function of distance and their averages (red squares) obtained by considering stations within 10, 30, 50…km. The expected average τ_c value from the τ_c vs. M relationship is represented by a blue dashed line.

Conclusions

The present work is aimed at testing the validity of the threshold-based method for earthquake early-warning systems. For such a purpose, the method has been applied to ten large Japanese earthquakes that occurred from 2000 to 2009, and an off-line simulation of the procedure has been performed for each event. The application of the method to the selected events confirmed the feasibility of using a threshold-based approach for early-warning procedures. The performance of the system has been evaluated by defining successful, missed, and false alarms (Table 2) and by counting their relative percentage. A very high percentage (~88%) of alert levels has been correctly assigned (Fig. 5), and most of the maximum alert levels correspond to the area within which the highest level of damage has been observed.

In this paper we propose a quantitative approach for a real-time mapping of the potential damage zone. The proposed methodology is based on the interpolation of measured and predicted values of peak ground displacement, which allows for a rapid estimation of the potential damage zone. The PDZ, delimited by the $P_d = 0.2$ cm isoline, is available within a few seconds from the origin time and generally becomes stable after about 10 s. Furthermore, as soon as local measurements are available at more distant sites, the extension of the PDZ can be refined and local alert levels can be used to validate the alert issued by near-source stations.

The studied cases displayed a very good agreement between the rapidly predicted and observed damage zone: the PDZ turned out to be very consistent with the area on I_{JMA} and I_{MM} maps in which the highest level of damage is reported. For the 2008, Iwate–Miyagi earthquake, we observed a large discrepancy between the PDZ and the observed damage zone. We infer that the anomalously large PDZ could be due to a low frequency attenuation effect in the northwest–north direction, which results in an overestimation of the potential damage zone.

The proposed methodology for earthquake early warning is suitable to Japan or other high–seismic risk countries worldwide, where a dense network of accelerometers is developed over the whole territory. Compared with the pure on-site and regional early-warning systems, this approach, based on interpolation of measured and observed peak displacement values, is likely to provide more robust prediction of potential earthquake damaging effects. A fast and reliable transmission system with small latency time is required, and efficient algorithms are necessary for a rapid processing of signals.

Data and Resources

Seismic data used in this study were collected from the KiK-net and K-NET on-line databases (http://www.kik.bosai.go.jp/ and http://www.k-net.bosai.go.jp/, last accessed October 2011).

Data analysis and some of the figures were made using GNUPLOT (http://www.gnuplot.info/, last accessed October 2011), SAC (Goldstein *et al.*, [2003], which can be requested from the Incorporated Research Institutions for Seismology at http://www.iris.edu, last accessed October 2011), and Generic Mapping Tools (Wessel and Smith, 1995; http://gmt.soest.hawaii.edu/, last accessed October 2011). The color palette used in Figure 4 was taken from the ShakeMap online manual (http://earthquake.usgs.gov/earthquakes/shakemap/, last accessed October 2011).

Acknowledgments

This work was financially supported by Dipartimento della Protezione Civile (DPC) through Analisi e Monitoraggio del Rischio Ambientale (AMRA, S.c. a r.l., Analysis and Monitoring of Environmental Risk) within the research contract REAC, by EU-FP7 in the framework of project REAKT and by project RELUIS 2011. We acknowledge the *Annual Bulletin of Japan (2008)*, published by the Japan Meteorological Agency (2010) for the intensity data. We also thank Drs. Mitsuyuki Hoshiba and Nobuo Hamada for making us available the JMA intensity data.

References

Alcik, H., O. Ozel, N. Apaydin, and M. Erdik (2009). A study on warning algorithms for Istanbul earthquake early warning system, *Geophys Res. Lett.* **36,** L00B05, doi 10.1029/2008GL036659.

Allen, R. M., and H. Kanamori (2003). The potential for earthquake early warning in southern California, *Science* **300,** 685–848.

Allen, R. M., H. Brown, M. Hellweg, O. Khainovski, P. Lombard, and D. Neuhauser (2009). Real-time earthquake detection and hazard assessment by ElarmS across California, *Geophys. Res Lett.* **36,** L00B08, doi 10.1029/2008GL036766.

Allen, R. M., P. Gasparini, O. Kamigaichi, and M. Böse (2009). The status of earthquake early warning around the world: An introductory overview, *Seismol. Res. Lett.* **80,** 682–693.

Böse, M., C. Ionescu, and F. Wenzel (2007). Earthquake early warning for Bucharest, Romania: Novel and revised scaling relations, *Geophys. Res. Lett.* **34,** doi 10.1029/2007GL029396.

Böse, M., E. Hauksson, K. Solanki, H. Kanamori, and T. H. Heaton (2009). Real-time testing of the on-site warning algorithm in southern California and its performance during the July 29 2008 M_{w} 5.4 Chino Hills earthquake, *Geophys. Res. Lett.* **36,** doi 10.1029/2008GL036366.

Espinosa-Aranda, J. M., A. Cuellar, A. Garcia, G. Ibarrola, R. Islas, S. Maldonado, and F. H. Rodriguez (2009). Evolution of the Mexican Seismic Alert System (SASMEX), *Seismol. Res. Lett.* **80,** 694–706.

Goldstein, P., D. Dodge, M. Firpo, and Lee Minner (2003). SAC2000: Signal processing and analysis tools for seismologists and engineers. Invited contribution to *The IASPEI International Handbook of Earthquake and Engineering Seismology*, W. H. K. Lee, H. Kanamori, P. C. Jennings, and C. Kisslinger (Editors), Academic Press, London.

Horiuchi, S., H. Negishi, K. Abe, A. Kamimura, and Y. Fujinawa (2005). An automatic processing system for broadcasting system earthquake alarms, *Bull. Seismol. Soc. Am.* **95,** 347–353.

Japan Meteorological Agency (2010). *The Annual Seismological Bulletin of Japan for 2008* (CD-ROM), Japan Meteorological Agency, Tokyo.

Kanamori, H. (2005). Real-time seismology and earthquake damage mitigation, *Annu. Rev. Earth Planet. Sci.* **33,** 195–214, doi 10.1146/annurev.earth.33.092203.122626.

Karim, K. R., and F. Yamazaki (2002). Correlation of JMA instrumental seismic intensity with strong motion parameters, *Earthq. Eng. Struct. Dynam.* **31,** 1191–1212.

Kunugi, T. (2000). Relationship between Japan Meteorological Agency instrumental intensity and instrumental modified Mercalli intensity obtained from K-NET strong-motion data, *Zisin* **54,** 89–93.

Nakamura, Y. (1984). *Development of earthquake early-warning system for the Shinkansen, some recent earthquake engineering research and practical in Japan*, The Japanese National Committee of the International Association for Earthquake Engineering, Tokyo, Japan, 224–238.

Nakamura, Y. (1988). On the Urgent Earthquake Detection and Alarm System (UrEDAS), in *Proceedings 9th World Conf. Earthquake Engineering*, 2–9 August 1988, Tokyo–Kyoto, Japan, Railway Technical Research Institute, **7,** 673–678.

Odaka, T., K. Ashiya, S. Tsukada, S. Sato, K. Ohtake, and D. Nozaka (2003). A new method of quickly estimating epicentral distance and magnitude from a single seismic record, *Bull. Seismol. Soc. Am.* **93,** 526–532.

Peng, H. S., Z. L. Wu, Y. M. Wu, S. M. Yu, D. N. Zhang, and W. H. Huang (2011). Developing a prototype earthquake early warning system in the Beijing capital region, *Seismol. Res. Lett.* **82,** 394–403.

Satriano, C., A. Lomax, and A. Zollo (2008). Real-time evolutionary earthquake location for seismic early warning, *Bull. Seismol. Soc. Am.* **98,** 1482–1494.

Satriano, C., L. Elia, C. Martino, M. Lancieri, A. Zollo, and G. Iannaccone (2010). PRESTo, the earthquake early warning system for southern Italy: Concepts, capabilities and future perspectives, *Soil Dynam. Earthq. Eng.* **31,** doi 10.1016/j.soildyn.2010.06.008.

Ueno, H., S. Hatakeyama, T. Aketagawa, J. Funasaki, and N. Hamada (2002). Improvement of hypocenter determination procedures in the Japan Meteorological Agency, *Q. J. Seismol.* **65,** 123–134.

Wald, D. J., V. Quitoriano, T. H. Heaton, and H. Kanamori 1999. Relationships between peak ground acceleration, peak ground velocity and modified Mercalli intensity in California, *Earthq. Spectra* **15,** 557–564.

Wessel, P., and W. H. F. Smith (1995). New version of the Generic Mapping Tools released, *Eos Trans. AGU* **76,** 329.

Wu, Y. M., and H. Kanamori (2005). Rapid assessment of damage potential of earthquake in Taiwan from the beginning of *P* waves, *Bull. Seismol. Soc. Am.* **95,** doi 10.1785/0120040193, 1181–1185.

Wu, Y. M., and H. Kanamori (2008). Development of an earthquake early warning system using real-time strong motion signals, *Sensors* **8,** 1–9.

Wu, Y. M., and T. L. Teng (2002). A virtual sub-network approach to earthquake early warning, *Bull. Seismol. Soc. Am.* **92,** 2008–2018.

Wu, Y. M., and L. Zhao (2006). Magnitude estimation using the first three seconds *P*-wave amplitude in earthquake early warning, *Geophys. Res. Lett.* **33,** L16312, doi 10.1029/2006GL026871.

Zollo, A., G. Iannaccone, M. Lancieri, L. Cantore, V. Convertito, A. Emolo, G. Festa, F. Gallovič, M. Vassallo, C. Martino, C. Satriano, and P. Gasparini (2009). Earthquake early warning system in southern Italy: Methodologies and performance evaluation, *Geophys. Res. Lett.* **36,** L00B07, doi 10.1029/2008GL036689.

Zollo, A., G. Iannaccone, V. Convertito, L. Elia, I. Iervolino, M. Lancieri, A. Lomax, C. Martino, C. Satriano, E. Weber, and P. Gasparini (2009). The earthquake early warning system in southern Italy, in *Encyclopedia of Complexity and System Science*, Vol. **5**, Springer, New York, doi 10.1007/978-0-387-30440-3, 2395–2421.

Zollo, A., O. Amoroso, M. Lancieri, Y. M. Wu, and H. Kanamori (2010). A threshold-based earthquake early warning using dense accelerometer networks, *Geophys. J. Int.* **183,** 963–974.

Dipartimento di Scienze Fisiche
Unità di Ricerca in Sismologia Sperimentale e Computazionale
Università degli Studi di Napoli, Federico II
Complesso Universitario di Monte S. Angelo, Via Cinthia
I-80126 Napoli, Italy
simona.colombelli@unina.it
(S.C., O.A., A.Z.)

California Institute of Technology
Seismological Laboratory
1200 E. California Blvd., MS-252 21
So. Mudd Building, Rm 263
Pasadena, California 91125
(H.K.)

Manuscript received 17 May 2011